LABORATORY EXPERIMENTS OF BICHROMATIC WAVE GROUPS PROPAGATION ON A GENTLE SLOPE BEACH PROFILE AND ENERGY TRANSFER TO LOW AND HIGH FREQUENCY COMPONENTS

Enrique M. Padilla[1] and José M. Alsina[1]

This work presents a first analysis of experimental data studying the influence of the frequency bandwidth on the propagation of bichromatic wave groups over a constant 1:100 beach slope. The use of a large spatial cross-shore resolution and Bi-Spectral analysis techniques allows the identification of nonlinear energy transfers along the propagation of wave groups. During wave-group shoaling, nonlinear coupling between the primary wave frequencies results in a larger growth of superharmonics for narrow-banded wave conditions, increasing the skewness of the wave and leading to eventual instabilities and earlier high frequency (hf) wave breaking compared to the broad-banded wave condition. Regarding the growth of low frequency (lf) component, the data analysis has shown a larger growth of the incident bound long wave (IBLW) for broad-banded wave conditions. It is generally assumed that the transferred energy from the primary wave components to subharmonics does not affect the short wave energy budget. Here, the opposite is hypothesised, and a larger growth of the IBLW for broad-banded wave conditions is accompanied of a larger reduction of the primary wave components, a reduced growth of hf components and, consequently, a reduction in the growth of hf wave asymmetry during wave group shoaling. Conversely for narrow-banded wave conditions, a reduced IBLW growth is associated with a larger growth of hf wave asymmetry. After hf wave breaking, within the low frequency domain (lf), the IBLW decays slightly for narrow-banded conditions, consistent with a reduction in radiation stress forcing. This involves a nonlinear energy transfer from the wave group frequency back to hf components. The remaining lf energy, Outgoing Free Long Wave (OFLW), reflects back at the shoreline. However, for broad-banded wave conditions, strong dissipation and minimal reflection of lf components occurs close to the shoreline, which might be caused by lf wave breaking.

Keywords: Grouping waves; Bandwidth; Energy transfer

INTRODUCTION

The grouping of hf waves and the presence of associated lf motions are characteristic features of random sea/swell wave conditions propagating to the coastline. During wave group shoaling, nonlinear coupling between primary frequency components causes a net energy transfer to those being subharmonics and superharmonic of the primary incident components. The growth of low and high frequency components during wave group shoaling has been traditionally treated separately in the literature although both mechanisms interplay.

Focusing on the wave grouping, a random sea state may be reduced to a bichromatic wave condition where the group modulation is performed by the combination of only two frequencies (primary components $\{f_1, f_2\}$). Essentially, the physical processes are all maintained and the nonlinear interactions between pairs of components cause energy transfers within the wave spectrum in the same way as it does in random sea states (*Phillips*, 1960; *Hasselmann et al.*, 1963). As wave groups shoal, resulting energy transfers come from the varying phase-coupling between the primary frequencies (*Herbers et al.*, 2000; *De Bakker et al.*, 2014, 2015). Higher Order Spectra (HOS), bispectral analysis in particular, may account for that phase coupling that eventually promotes the enhancement of the third component in the triad. This third one might be above (hf) or below (lf) the primary interacting frequencies depending on the nature of the interaction (sum, difference and self interactions). These are higher order waves well known for not evolving as free waves. For instance, the incoming bound long wave (IBLW) at the grouping frequency f_g comes from the difference-interaction between $\{f_1, f_2\}$ and results in a group-bound long wave antiphase-locked with the envelope of the primary waves (*Longuet-Higgins and Stewart*, 1962).

The growth of this incident low frequency components bounded to the wave groups during shoaling has been reported (*Baldock et al.*, 2000; *Battjes et al.*, 2004; *Van Dongeren et al.*, 2007). In the shoaling process, the IBLW gains energy at the expense of the short wave energy. Usually, the resulting loss of energy from the short waves is assumed to be small in comparison to the total short wave energy and not considered. The process of bound wave growth during hf wave group shoaling is associated to an additional phase shift over the 180° phase lag between the wave group envelope and the IBLW (*List*, 1992; *Van Dongeren and Svendsen*, 1997; *Baldock et al.*, 2000; *Janssen et al.*, 2003; *Battjes et al.*, 2004). *Battjes et al.* (2004), empirically computed the energy transfer from the hf group envelope to the IBLW during wave groups shoaling. Two scenarios are illustrated depending of the value of the dimensionless

[1]Department of Civil and Environmental Engineering, Imperial College of London, United Kingdom

normalized bed slope parameter β (*Battjes et al.*, 2004): a "mild-slope" regime where the beach slope is gentle compared to the group frequency and the IBLW amplitude growth is well approximated to be proportional to $h^{-5/2}$ (being h the water depth); and a "steep-slope" regime where the beach slope is relatively steep compared to the bound wave frequency and the energy transfer mechanism is less efficient. In this case, the growth of the IBLW is shown to be proportional to $h^{-1/4}$ (Greens's law).

A number of experimental and field data sets suggest that IBLWs follow strong near-shore dissipation after wave group breaking (*Baldock et al.*, 2000; *Battjes et al.*, 2004; *Henderson et al.*, 2006; *Baldock*, 2012). The aforementioned dimensionless parameter β, also controls the near-shore behaviour of lf–motions. For some lf components and beach slope S combinations resulting in small values of β, the dissipation of lf waves close to the shoreline is attributed to long wave breaking (*Battjes et al.*, 2004; *Van Dongeren et al.*, 2007; *De Bakker et al.*, 2014), which suggests lf energy saturation at the shoreline. *Battjes et al.* (2004) found that lf reflection at the shoreline was small for low values of β (mild-slope regime). Hence, they also suggested that the observed lf energy losses are due to long wave breaking. Laboratory data have confirmed that with decreasing depth the lf wave self-self interaction may dominate energy transfer causing the lf wave front to steepen up and eventually break (*Van Dongeren et al.*, 2007). This seems consistent with field measurements of run-up elevation (*Ruessink et al.*, 1998; *Sénéchal et al.*, 2011) showing run-up energy saturation at lf domain during highly dissipative energetic storms. However, near-shore lf wave dissipation has been also suggested to occur through nonlinear interaction that transfer energy from the lf waves back to hf components and it is not generally attributed to frictional losses (*Henderson et al.*, 2006).

The growth of high frequency components during shoaling influencing wave skewness and asymmetry has been also studied in several works (*Elgar and Guza*, 1985, 1986; *Doering and Bowen*, 1986; *De Bakker et al.*, 2015). It is well known that the enhancement of the high order components results in a change of the waves forming the wave groups. From a quasi symmetrical profile in deep waters, the surface elevation evolves to more skewed waves in shallow waters characterized by sharp crests and flat broad troughs. The pitching forward of the individual waves, or relative steepening of the wave face, represents a forward phase-shifting of the harmonics relative to the primary components (*Elgar and Guza*, 1986; *Doering and Bowen*, 1986, 1995). These nonlinearities of hf waves propagating across a natural beach are important to sediment transport (*Ruessink et al.*, 2009) or to the design of coastal structures and wave loads computation. Ignoring any other forcing, the depth-induced wave-asymmetry itself may be eventually responsible for the hf wave breaking although evidences of a relationship between nonlinear energy transfer and wave breaking has been establish to our best knowledge. After hf wave breaking, the remaining hf energy still drives water oscillations to the shoreline. However, due to hf energy dissipation during breaking, the wave energy close to the shoreline may be dominated by lf wave motions, specially in dissipative beach conditions. The presence of this lf energy is particularly important at the operability and safety of coastal infrastructures such as harbours (*Bowers*, 1977) and erosion of beaches(*Russell*, 1993).

The main aim of this work is to study the wave group propagation in highly dissipative beach conditions, i.e. a beach slope of 1:100, and the energy transfer from primary waves to superharmonics and subharmonics due to nonlinear frequency coupling (triad interactions). Bichromatic wave groups cases have been generated in laboratory conditions, and the energy transfer between frequency components during wave group propagation studied using Bispectral techniques.

MATERIAL AND METHODS

Experimental set-up

The experiments presented in this study have been carried out in the Wave-Evolution Flume at Imperial College London. This is a glass-made wave flume with a length of 60 m whose distance from the paddles to the emerged end is of nearly 52 m. The flume width is 0.3 m with a working water depth of 0.5 m. A near-shore area under dissipative conditions is available due to the existence of a beach profile, made of solid glass, with a gentle slope (1:100). The water surface elevation measuring system is composed by a set of resistance-type gauges (RTG) and acoustic-type sensors (ATS). The setup of both systems allow us to obtain a surface elevation data set with a spatial resolution from 0.3 m in the shoaling zone to 0.1 m in the surf zone. The acoustic-type sensors are used in the downstream end of the flume within the swash zone. The designed spatial resolution provided by those instruments is presented in Figure 1 over a flume sketch.

The waves are generated using a flat-backed, bottom-hinged, wave paddle which is numerically con-

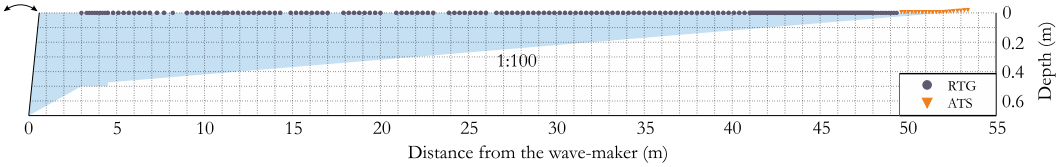

Figure 1: Cross-shore bottom profile, still water level and instrument locations deployed from the wave paddles. The presented positions perform the overall locations of the resistive-type (dots) and acoustic-type gauges (triangles) across the repetitive runs.

trolled with active force feedback. This guarantees the generation of the desired waves and the absorption of any unwanted reflected wave. Wave generation is performed using a Force Control technique that has been shown to be effective suppressing high frequency spurious (*Spinneken and Swan*, 2011). This technique is included in the commercial software that controls the wave paddle. The software does not allow for second order wave generation. However, for this study, we introduced an active suppression system of spurious subharmonics in the form of unwanted energy as free incident long waves. The suppression technique proceeds as follows and it is based on the separation procedure explained below. After an initial generation, any incident free lf wave motion (spurious) is separated using measured time series of water surface elevation at different cross-shore locations. After back propagation to the wave paddle, a correction is introduced to suppress the unwanted free incident component during generation. This methodology provides in practice the same result than theoretical second order transfer functions with the inconvenient of having measured and effectively computed the correction each time.

Dataset description

In this work, we show 2 bichromatic wave cases with the same energy content and energy flux, whose main difference is the bandwidth. These are fully-modulated cases ($a_1/a_2 = 1$) with the same initial amplitude for the primary frequencies ($a_1 = a_2 = 0.015$ m). The mean primary frequency, $f_p = (f_1 + f_2)/2$, is intentionally kept the same and the wave group frequency is varied by modifying the bandwidth ($f_g = f_1 - f_2$). The selection of the specific bandwidths presented in table 1 is such that the hf waves synchronise the phase exactly at every group period, in other words, the groups are identical each other. Consequently, based on this specific condition, f_g is computed in terms of the number of short waves n forming the group:

$$f_g = \frac{f_p}{n + 1/2}. \tag{1}$$

The highest bandwidth (0.171 Hz) corresponds to the shorter case, composed by 3 wave-crests. In contrast, the longest wave group, with 12 wave-crests, yields a bandwidth of 0.048 Hz. The designed experiments are characterized by 12 minutes time-length data series with a sampling frequency of 100 Hz.

IBLW separation technique for field data

Assuming a second-order theory description of the free surface elevation, η_{f_g} represents the lf component at the group frequency. It is described by:

$$\eta_{f_g}(x,t) = \Re\left\{\left[\left(Z^{IBLW}\, e^{-i(k_{IBLW}\, x)}\right) + \left(Z^{+}\, e^{-i(k\, x)}\right) + \left(Z^{-}\, e^{i(k\, x)}\right)\right] e^{i(2\pi f_g\, t)}\right\}, \tag{2}$$

where the superscripts (+) and (−) refer to the incoming or outgoing nature of the free waves and Z is a complex amplitude that includes the amplitude and initial phase as $Z = A\, e^{i\,\phi_0}$. Therefore, separation is properly achieved once $Z^{\pm}$ and Z^{IBLW} are computed.

For this purpose, the separating methodology follows the approach proposed by *Battjes et al.* (2004), extended to the existence of an ingoing free wave. It consists on separating those 3 waves at any location x_r

Table 1: Bichromatic wave-group series

Case	f_p (Hz)	f_1 (Hz)	f_2 (Hz)	f_g (Hz)	n	$N(a_1/a_2)$	a_1 (m)
n03	0.6	0.686	0.514	0.171	3	1	0.015
n12	0.6	0.624	0.576	0.048	12	1	0.015

(reference location) by solving a system that involves local wave data from adjacent positions x_p. Working in the frequency domain, that system is defined as:

$$Z_p = Q_{rp}^{IBLW} Z_r^{IBLW} + Q_{rp}^{+} Z_r^{+} + Q_{rp}^{-} Z_r^{-}, \tag{3}$$

where $Q_{rp} = K_{rp} \cdot e^{i \cdot \Phi_{rp}}$ and represents the propagation coefficient from x_r to every single location x_p. K and Φ are factors that perform the evolution of the amplitude and the phase, respectively, based on the nature of the wave.

For free waves, the amplitude evolves following the Green's Law and the phase includes the depth-induced variations in the wave celerity c:

$$K_{rp}^{\pm} = (h_r/h_p)^{1/4}, \tag{4}$$

$$\Phi_{rp}^{\pm} = \mp 2\pi f_g \int_{x_r}^{x_p} \frac{1}{c} dx. \tag{5}$$

However, the IBLW requires particular considerations. Its growth is assumed to follow a function of the local depth raised to a power α, whose initial guess value is the corresponding one to the best fit over the whole wave-height at f_g. Otherwise, the phase evolves following the linear theory group velocity at the mean frequency of the primary waves, c_{gp}:

$$K_{rp}^{IBLW} = (h_r/h_p)^{\alpha}, \tag{6}$$

$$\Phi_{rp}^{IBLW} = -2\pi f_g \int_{x_r}^{x_p} \frac{1}{c_{gp}} dx. \tag{7}$$

Considering a solving array composed by P locations, the overdetermined version of the system presented in Equation (3) is:

$$\begin{pmatrix} Q_{p_1}^{IBLW} & Q_{p_1}^{+} & Q_{p_1}^{-} \\ Q_{p_2}^{IBLW} & Q_{p_2}^{+} & Q_{p_2}^{-} \\ \vdots & \vdots & \vdots \\ Q_{p_n}^{IBLW} & Q_{p_n}^{+} & Q_{p_n}^{-} \end{pmatrix} \begin{pmatrix} Z_r^{IBLW} \\ Z_r^{+} \\ Z_r^{-} \end{pmatrix} = \begin{pmatrix} Z_{p_1} \\ Z_{p_2} \\ \vdots \\ Z_{p_n} \end{pmatrix}. \tag{8}$$

The separation implemented in this work uses a local array composed by 21 gauges whose mean separation is 30 cms. Specific configurations of the local array must be considered in order to avoid problems with singularities or numerical instabilities. The separation technique is computed twice using the system (8). In the first computation, the value of α in Equation (6) is obtained from the best fit over the wave height at f_g along the whole cross-shore domain. The separated IBLW in the first computation is immediately used to re-compute α and a proper separation of the IBLW is achieved after the second computation.

Nonlinear energy transfers based on HOS analysis

During wave propagation, the energy content associated to any frequency may either increase-decrease due to energy transfers among components or, just being reduced by dissipative processes. As a result, there is a net exchange of energy associated to a frequency f. This is presented as a balance between the cross-shore gradient of the energy flux spectrum $F_{x,f}$, a nonlinear source $S_{nl,f}$ computed by bispectral analysis and a dissipation term $S_{ds,f}$ that includes energy loses such as wave breaking:

$$\frac{\partial F_f(x)}{\partial x} = S_{nl,f}(x) + S_{ds,f}(x). \tag{9}$$

In this work, we will just focus on the nonlinear source term, which may be studied on the basis of high order spectral (HOS) to perform the nonlinear wave interactions (*Hasselmann et al.*, 1963; *Elgar and Guza*, 1985; *Herbers et al.*, 2000; *De Bakker et al.*, 2015, among others). Within the HOS techniques, the Bispectrum decomposes the third-order moment of a signal and analyses the interaction between frequency components in a triad $[f_i, f_j, f_i + f_j]$, accounting for their phases coupling:

$$B(f_i, f_j) = E[A_{f_i}^{*} A_{f_j}^{*} A_{f_i+f_j}], \tag{10}$$

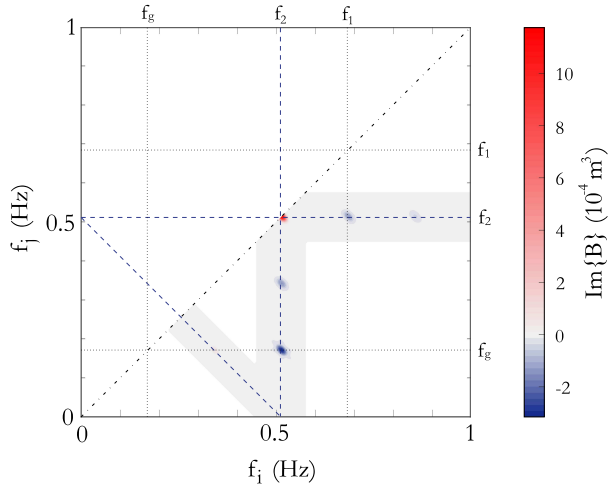

Figure 2: Imaginary part of the bispectrum of the incoming wave signal for the case *n03* at the location $x = 14.60$ m. The shaded area represents the symmetric half of the integration area that accounts for the energy balance based on Equation (11) for the component $f = f_2$.

where A refers to their complex Fourier coefficients. In the existing literature about HOS, there is another definition for the Bispectrum (both commented in *Collis et al.* (1998)) depending on which of the coefficients the complex conjugation ($*$) is affecting to. This later one is $\hat{B}(f_i, f_j) = E[A_{f_i} A_{f_j} A^*_{f_i+f_j}]$ and it is clear that the difference between those is that $\Im(B) = -\Im(\hat{B})$, where $\Im$ represents the imaginary part. Thus, in contrast to the definition presented by *De Bakker et al.* (2015), we will use the above one (Equation (10)) which is consistent with the usual sign criterion used for computing energy transfers based on bispectral analysis.

Physically, the energy transfer among a triad is assumed to be governed by the phase-relationship between these three interacting component, that is, the bispectrum. The linking equation between the energy transfer and triad interactions is

$$S_{nl,f} = 3\pi \frac{\rho g f}{h} \Im \left\{ \sum_{f'=0}^{f} B(f', f - f') - 2 \sum_{f'=0}^{f} B(f', f) \right\}, \tag{11}$$

where h is the water depth and $S_{nl,f}$ is the nonlinear source term that accounts for the energy transfers to (+) and from (-) a frequency f. This solution proposed by *Herbers and Burton* (1997) is based on the Boussinesq approach valid in shallow water during both shoaling and breaking short wave conditions. Since the sum terms in Equation (11) includes all possible interactions between triad constituent components, a representation in the symmetrical plane $f_i f_j$ (Figure 2) provides a graphical meaning and where non-zero combinations are expected. For a certain frequency f, its energy balance (Equation (11)) may be seen as proportional to the integration of the imaginary part of the bispectrum along the shaded area in Figure 2, turning over the sign for either $f_i = f$ or $f_j = f$ (the vertical and horizontal segments, associated to the term $\sum_{f'=0}^{f} B(f', f)$). Actually, this change of the sign comes from its physical interpretation: Assuming $\eta(t)$ composed by an energetic triad $[f_1, f_2, f_1 + f_2]$, if $\Im\{B(f_1, f_2)\} > 0$, f_1 and f_2 export energy to $f_1 + f_2$. In reverse, if $\Im\{B(f_1, f_2)\} < 0$, f_1 and f_2 receive energy from $f_1 + f_2$.

RESULTS AND DISCUSSION

Figures 3 and 4 gather the spatial evolution of the high and low frequency components for a broad- and narrow-banded bichromatic wave train, respectively. For a general view, panel *a* (Figure 3 and 4) shows a cross-shore evolution of the frequency spectral distribution. Close to the generation boundary, most of the spectral energy is concentrated on the target primary frequencies (f_1 and f_2), around $f_p = 0.6$ Hz. During shoreward wave propagation, higher order components progressively arise in high and low frequency domains. Whereas super-harmonics grow quickly during short waves shoaling, they also dissipate faster during hf wave breaking (from the dashed black line and forward). After breaking, the

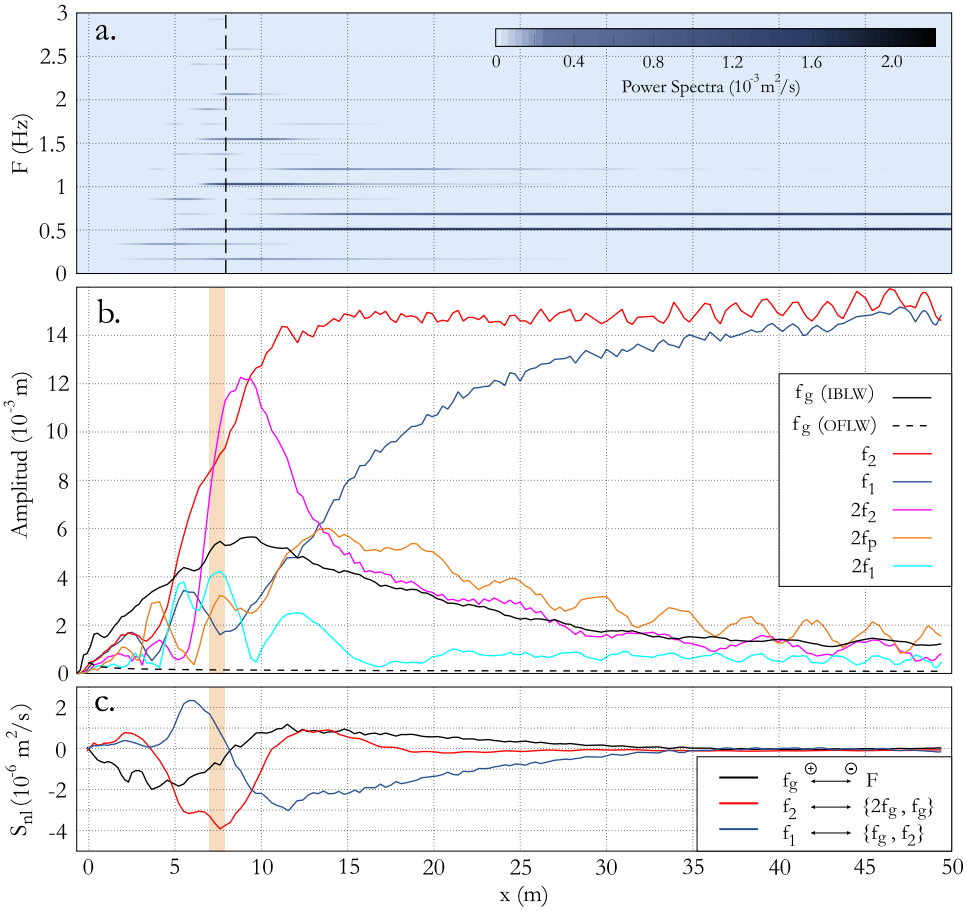

Figure 3: Panel *a* shows the cross-shore distribution of power spectra density at different frequency components for the case *n03*. Panel *b* gathers the cross-shore amplitude evolution of components belonging to the high and low frequency domain and panel *c* presents the energy fluxes to(+)/from(-) the primary waves to the rest of their triads; and to(+)/from(-) the IBLW to the rest of the frequency domain *F*.

remaining energy is mainly driven by the difference term at the group frequency ($f_g = f_1 - f_2$), which is the dominant among the sub-harmonic components.

Panel *b* presents the cross-shore amplitude evolution for the high and low frequency components compared to the evolution of the primary components, f_1 and f_2. The primary components initially concentrate more than 98 % of the spectral energy content and progressively decrease as they travel and transmit energy to higher and lower frequency components. For the broad-banded condition (Figure 3) and within the hf domain, the higher growth is in general observed by the self-self interaction component of f_2 ($\{f_2, f_2\} \rightarrow 2f_2$), whose maximum is reached just before the outer breaking location. At the same time, the energy budget associated to $2f_1$ remains remarkably low compared to $2f_2$, whereas the sum term $2f_p$ reaches it maximum growth far outside the surf zone. Likewise, in the lf domain, the IBLW grows significantly during hf groups shoaling, reaching a maximum energy content at the outer breaking location, far outside the shallow water limit. After hf wave breaking, the lf energy is progressively reduced until being almost completely dissipated at the shoreline.

The narrow-banded condition (*n12*) illustrated in Figure 4 shows some similarities compared to Figure 3. There are small differences in the growth of $2f_p$ component which presents a maximum close to the surf zone, a slightly less growth of $2f_2$ and also slightly larger growth of $2f_1$ for the narrow-banded case. However, the most distinguishing feature is a significantly smaller decay of f_1 component (f_2 also shows a slightly smaller decay), which has been already observed in previous works (*Baldock et al.*, 2000; *Alsina et al.*, 2016). In the low frequency domain, a smaller growth of the IBLW compared to the broad-banded case is observed. Furthermore, the IBLW does not reach a clear maximum in the surf zone as the

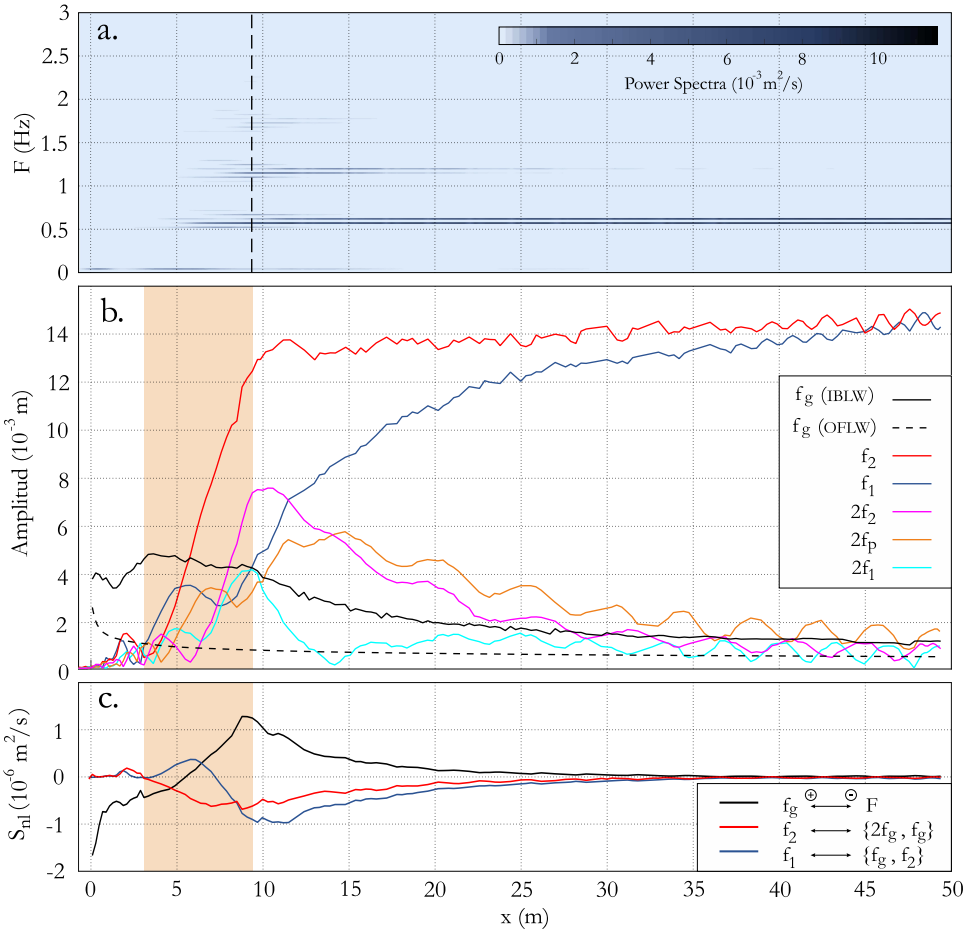

Figure 4: Panel *a* shows the cross-shore distribution of power spectra density at different frequency components for the case *n12*. Panel *b* gathers the cross-shore amplitude evolution of components belonging to the high and low frequency domain and panel *c* presents the energy fluxes to(+)/from(-) the primary waves to the rest of their triads; and to(+)/from(-) the IBLW to the rest of the frequency domain *F*.

broad-banded wave condition does and a high percentage of energy is reflected back at the shoreline.

Panel *c* shows the nonlinear energy balance over the components in the triad [f_g, f_2, f_1]. These energy exchanges spatially vary during wave propagation and depending of the frequency components involved. Positives fluxes mean that f_g, f_1 and f_2 receive energy, whereas negative ones imply a transfer from those to the rest of the triad. Particularly, the balance over f_g accounts for the resultant balance throughout all the triad interactions where f_g is involved (the whole frequency domain F). Regardless the bandwidth, it may be seen that f_1 component (blue line) is always the main energy supplier and responsible for the IBLW enhancement for both cases, but not in the same rate (see Figure 3–*c* and 4–*c*). For the case *n*12, f_1 and f_2 contribute similarly (slightly more from f_1) to the IBLW growth. The maximum combined $\langle f_1, f_2 \rangle$ contribution is reached at the outer breaking location but after that, they still supply energy with a lower rate which explains a gentle IBLW growth along the surf zone. In reverse, Figure 3 shows how the IBLW growth is almost entirely assumed by the component f_1. According to this, the maximum IBLW amplitude is reached at the same place where f_1 suffers the highest transference for the broad-banded wave condition. Moreover, The differential transfer of energy from the primary frequencies to the lf domain seems to explain the selective loss of energy for f_1 compared to f_2 as previously reported by *Baldock et al.* (2000) and *Alsina et al.* (2016).

The nonlinear coupling and energy transfer between components during wave groups shoaling and the bandwith influence explained above is reflected in the growth of the group frequency components f_g and high frequency components (harmonics and superharmonics). Figure 5 illustrates the bandwith influence

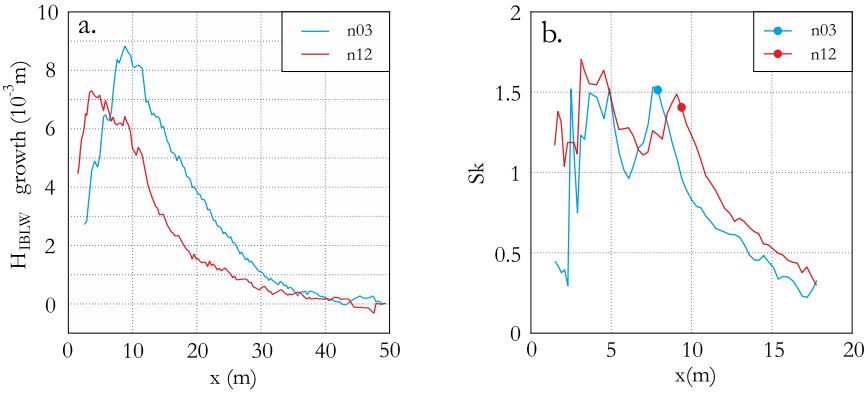

Figure 5: Cross-shore distributions of both the IBLW height growth (panel *a*) and the hf wave skewness (panel *b*), for the cases *n03* and *n12*.

on the IBLW growth during wave group shoaling (Fig. 5–*a*) and on the hf wave horizontal asymmetry (Skewness) growth (Fig. 5–*b*) during wave group propagation. The Skewness, Sk is computed as the normalized third moment of the hf water surface elevation η:

$$Sk = \frac{E[\eta^3(t)]}{E[\eta^2(t)]^3/2}, \tag{12}$$

where the normalizing factor $E[\eta^2(t)]^{3/2} = \sigma_\eta^3$ and the third moment is computed through bispectrum B (*Hasselmann et al.*, 1963) as

$$E[\eta^3(t)] = \int_{-\infty}^{+\infty}\int_{-\infty}^{+\infty} \Re\left\{B(f_i, f_j)\right\} df_i df_j. \tag{13}$$

The growth of the IBLW height during shoaling is computed as the difference between the measured IBLW at any cross-shore location with respect to the IBLW height at generation (Fig. 5–*a*). It is observed a larger IBLW energy increase for broad band wave conditions as a result of the differences in non-linear energy transfer and a larger contribution from f_1 for the broad band wave conditions. Conversely, the cross-shore distribution of the hf wave skewness shows an earlier growth of Skewness for narrow-banded conditions associated with an earlier hf wave breaking.

CONCLUSION

In this work, 2 different wave-group conditions have been generated, and their propagation over a gentle beach profile (1:100) have been studied experimentally. These are fully modulated bichromatic wave groups with the same energetic content and same primary wave frequency. The wave group frequency f_g was modified by varying the bichromatic bandwidth. Moreover, the high cross-shore wave-gauge resolution enabled a detailed analysis of nonlinear energy transfer between frequency components over a very long shoaling region. Hence, a first approach of the influence of the bandwidth over the hf and lf wave dynamics under dissipative conditions has been presented.

Preliminary results have shown a larger growth of high frequency components for narrow-banded wave conditions, increasing the skewness of the hf waves and leading to eventual instabilities and earlier high frequency (hf) wave breaking compared to the broad-banded wave condition. The presented data suggest a close relationship between the breaking events and the nonlinear energy transfers from the primary wave components to superharmonics. Hence, future work will focus on the implications of the grouping structure over the breaking event.

On the low frequency domain, the data analysis has shown a larger growth of the incident bound long wave (IBLW) for broad band wave conditions. In addition, evidences on the reduction in lf amplitudes close to the shoreline are shown. This preliminary analysis suggest an important influence of the wave group frequency and the beach slope. For the larger wave group frequency, the experimental data seems to support the lf breaking mechanism proposed by *Battjes et al.* (2004) and *Van Dongeren et al.* (2007), since

it might not be explained by nonlinear frequency interactions. However, the lower wave group frequency suggest nonlinear energy transfers to high frequency components and full reflection of the remaining low frequency energy at the shoreline as suggested by *Henderson et al.* (2006).

ACKNOWLEDGEMENTS

The first author is supported with a PhD fellowship from the Department of Civil and Environmental Engineering, Imperial College London.

References

Alsina, J. M., Padilla, E. M., and Cáceres, I. (2016). Sediment transport and beach profile evolution induced by bi-chromatic wave groups with different group periods. *Coastal Engineering* 114, 325–340.

Baldock, T. E., Huntley, D. A., Bird, P. A. D., O'Hare, T., and Bullock, G. N. (2000). Breakpoint generated surf beat induced by bichromatic wave groups. *Coastal Engineering* 39, 213–242.

Baldock, T. E. (2012). Dissipation of incident forced long waves in the surf zone – Implications for the concept of "bound" wave release at short wave breaking. *Coastal Engineering* 60, 276–285.

Battjes, J. A., Bakkenes, H. J., Janssen, T. T., and Van Dongeren, A. R. (2004). Shoaling of subharmonic gravity waves. *Journal of Geophysical Research: Oceans* 109(C2).

Bowers, E. C. (1977). Harbour resonance due to set-down beneath wave groups. *Journal of Fluid Mechanics* 79, 71–92.

Collis, W. B., White, P. R., and Hammond, J. K. (1998). Higher-order spectra: the bispectrum and trispectrum. *Mechanical systems and signal processing* 12(3), 375–394.

De Bakker, A. T. M., Tissier, M. F. S., and Ruessink, B. G. (2014). Shoreline dissipation of infragravity waves. *Continental Shelf Research* 72, 73–82.

De Bakker, A. T. M., Herbers, T. H. C., Smit, P. B., Tissier, M. F. S., and Ruessink, B. G. (2015). Nonlinear infragravity–wave interactions on a gently sloping laboratory beach. *Journal of Physical Oceanography* 45(2), 589–605.

Doering, J. C., and Bowen, A. J. (1986). Shoaling surface gravity waves: A bispectral analysis. *Proc. 20th Int. Conf. Coastal Engineering*, 150–162.

Doering, J. C., and Bowen, A. J. (1995). Parametrization of orbital velocity asymmetries of shoaling and breaking waves using bispectral analysis. *Coastal Engineering* 26(1), 15–33.

Elgar, S., and Guza, R. T. (1985). Observations of bispectra of shoaling surface gravity waves. *Journal of Fluid Mechanics* 161, 425–448.

Elgar, S., and Guza, R. T. (1986). Nonlinear model predictions of bispectra of shoaling surface gravity waves. *Journal of Fluid Mechanics* 167, 1–18.

Hasselmann, K., Munk, W., and MacDonald, G. (1963). Bispectra of ocean waves. *Time series analysis*, 125–139.

Henderson, S. M., Guza, R. T., Elgar, S., Herbers, T. H. C., and Bowen, A. J. (2006). Nonlinear generation and loss of infragravity wave energy. *Journal of Geophysical Research: Oceans*, 111(C12).

Herbers, T. H. C., and Burton, M. C. (1997). Nonlinear shoaling of directionally spread waves on a beach. *Journal of Geophysical Research: Oceans* 102(C9), 21101–21114.

Herbers, T. H. C., Russnogle, N. R., and Elgar, S. (2000). Spectral Energy Balance of Breaking Waves within the Surf Zone. *Journal of physical oceanography* 30(11), 2723–2737.

Janssen, T. T., Battjes, J. A., and Van Dongeren, A. R. (2003). Long waves induced by short-wave groups over a sloping bottom. *Journal of Geophysical Research: Oceans*, 108(C8).

List, J. H. (1992). A model for the generation of two-dimensional surf beat. *Journal of Geophysical Research: Oceans* 97(C4), 5623–5635.

Longuet-Higgins, M. S., and Stewart, R. W. (1962). Radiation stress and mass transport in gravity waves, with application to 'surf beats'. *Journal of Fluid Mechanics* 13, 481–504.

Phillips, O. M. (1960). On the dynamics of unsteady gravity waves of finite amplitude Part 1. The elementary interactions. *Journal of Fluid Mechanics* 9, 193–217.

Ruessink, B. G., Kleinhans, M. G., and den Beukel, P. G. L. (1998). Observations of swash under highly dissipative conditions. *Journal of Geophysical Research: Oceans* 103(C2), 3111–3118.

Ruessink, B. G., Van den Berg, T. J. J., and Van Rijn, L. C. (2009). Modeling sediment transport beneath skewed asymmetric waves above a plane bed. *Journal of Geophysical Research: Oceans*, 114(C11).

Russell, P. E. (1993). Mechanisms for beach erosion during storms. *Continental Shelf Research*, 13(11), 1243-1265.

Sénéchal, N., Coco, G., Bryan, K. R., and Holman, R. A. (2011). Wave runup during extreme storm conditions. *Journal of Geophysical Research: Oceans*, 116(C7).

Spinneken, J., and Swan, C. (2011). Theoretical transfer function for force-controlled wave machines. *International Journal of Offshore and Polar Engineering*, 21(03).

Van Dongeren, A. R., and Svendsen, I. A. (1997). Quasi 3-D modeling of nearshore hydrodynamics (No. CACR-97-04). *Cent. for Appl. Coastal Res., Univ of Delaware, Nemark.*

Van Dongeren, A. R., Battjes, J., Janssen, T. T., Van Noorloos, J., Steenhauer, K., Steenbergen, G., and Reniers, A. J. H. M. (2007). Shoaling and shoreline dissipation of low-frequency waves. *Journal of Geophysical Research: Oceans*, 112(C2).